Investigation of Hybrid EMI Filters for Common-Mode EMI Suppression in a Motor Drive System

Shuo Wang, *Senior Member, IEEE*, Yoann Yorrick Maillet, Fei (Fred) Wang, *Fellow, IEEE*, Dushan Boroyevich, *Fellow, IEEE*, and Rolando Burgos, *Member, IEEE*

***Abstract*—This paper begins with an analysis of the common-mode (CM) noise in a motor drive system. Based on the developed CM noise model, two cancellation techniques, CM noise voltage cancellation and CM noise current cancellation, are discussed. The constraints and impedance requirements for these two cancellation methods are investigated. An active filter with a feedforward current cancellation technique is proposed, implemented, and tested, and techniques to improve the performance of active filters are explored. It is found that due to the limitations of speed, power loss, and gain bandwidth of active filters, active electromagnetic interference (EMI) filters are not good at suppressing high di/dt or high amplitude noise current. Hybrid filters that include a passive filter and an active filter are proposed to overcome the shortcomings of active filters. Hybrid EMI filters are investigated based on the impedance requirements and frequency responses between the passive and active filters. The experiments show that the proposed active filter can greatly reduce noise by up to 50 dB at low frequencies (LFs), and therefore, the corner frequency of the passive filter can be increased considerably; as a result, the CM inductance of the passive filter is greatly reduced. The power loss of the proposed active EMI filter can be well-controlled in the experiments.**

***Index Terms*—Active electromagnetic interference (EMI) filter, common-mode (CM) noise, current-controlled current source, hybrid EMI filter, motor drive.**

I. Introduction

SWITCHING-MODE power conversion systems generate conducted electromagnetic interference (EMI) noise, which flows within power-feeding paths, and between the power conversion systems and the ground. The noise flowing within the power-feeding paths is usually called differential-mode (DM) noise, and the noise flowing between the power conversion system and the ground is usually called common-mode (CM) noise. Passive EMI filters, which include both CM and DM filters, are usually used to attenuate both CM and DM noise. In CM filters, the CM capacitance of CM capacitors is usually limited by safety standards, which specify the maximum leakage current allowed to flow to the ground. Since the CM capacitance is limited by the leakage current, CM inductance could be as large as several millihenries to achieve enough noise attenuation in practical applications. Since the CM inductor must carry the full load current, its size is very big in high-power applications. In some applications, the leakage of the CM inductor is used as the DM inductance for DM filters. However, mutual parasitic couplings can be a problem [1]–[3]. Furthermore, the leakage of the CM inductor is usually very small, so DM inductance may not be large enough to achieve the required noise attenuation. Separate DM inductors are, therefore, used in many applications. The sizes of DM capacitors can be big, since their capacitance should be large enough to have low impedance to efficiently bypass noise and handle a high ripple current. The capacitor may also need to have a high-voltage rating for many applications. For motor drive systems, the switching frequencies are usually not high, for example, below 20 kHz. EMI standards, such as MIL-STD-461E and CISPR 11, concern EMI noise starting from 10 kHz. Therefore, the corner frequencies of EMI filters are usually below 10 kHz. Because of these, the sizes of passive EMI filters are usually very big. In some applications, passive EMI filters can take up to half of the size of a motor drive system. In order to reduce the size of the whole system, the use of active EMI filters to reduce EMI noise has been discussed in [5]–[11]. Ogasawara *et al.* [5] proposed a CM noise voltage cancellation method using a coupled inductor on the output of a motor drive. Julian *et al.* [6] proposed a method to reduce CM noise by adding a fourth phase leg to the motor drive with a new modulation scheme. Viability of active EMI filters for utility applications is analyzed in [8]. Active filters for ripple reduction in dc/dc converters were designed in [9]. A nullification process is followed in [10] to design active ripple filters. A hybrid EMI filter that includes a planar passive filter and an active filter is analyzed and simulated in [7] for planar TV applications. Hybrid ripple filters employing current injection or voltage injection are evaluated and implemented for dc/dc converters in [11] and [12]. These publications are very important to power electronics and EMI research.

Manuscript received March 12, 2009; revised May 22, 2009 and August 2, 2009. Current version published April 14, 2010. This work was supported by the SAFRAN Group, by the National Science Foundation under NSF Award Number EEC-9731677, and by the Center for Power Electronics Systems Industry Partnership Program. Recommended for publication by Associate Editor P. Tenti.

S. Wang is with the Electrical Power Systems, GE Aviation, Vandalia, OH 45377 USA (e-mail: shuowang@ieee.org; shwang6@vt.edu).

Y. Y. Maillet is with the Converteam, Inc, Pittsburg, PA 15238-2907 USA.

F. (Fred) Wang is with the Department of Electrical Engineering and Computer Science, University of Tennessee, Knoxville, TN 37996-2100 USA.

D. Boroyevich is with the Department of Electrical and Computer Engineering, Virginia Polytechnic Institute and State University, Blacksburg, VA 24061 USA.

R. Burgos is with the U.S. Corporate Research Center, ABB, Inc., Raleigh, NC 27606 USA.

Color versions of one or more of the figures in this paper are available online at http://ieeexplore.ieee.org.

Digital Object Identifier 10.1109/TPEL.2009.2033601

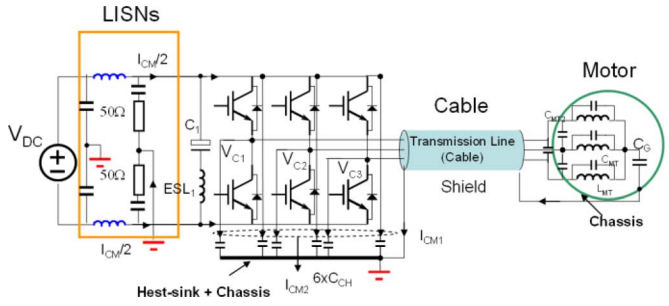

Fig. 1. Motor drive system with CM parasitic capacitance.

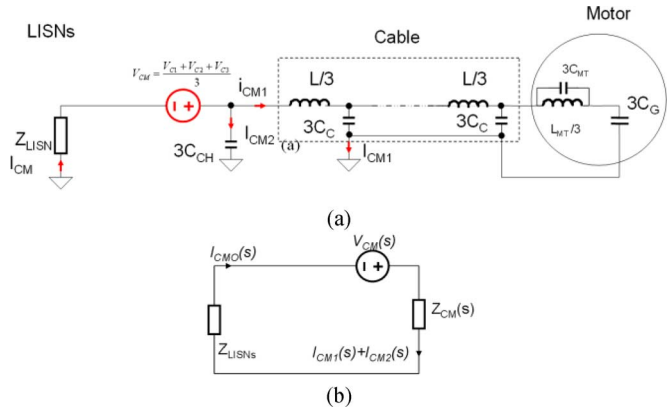

Fig. 2. CM noise model of a motor drive system. (a) Noise model. (b) Equivalent circuit.

For a hybrid EMI filter, the active filter part should be designed to attenuate LF noise. The inductance and capacitance of the passive filter can be reduced, since the corner frequency of the passive filter is to be increased after the active filter suppresses LF EMI. The size of the passive filter can therefore be reduced. The active filter can be implemented with the main control circuits in the system. They can also be integrated into an IC, and therefore, they do not take up much space.

This paper investigates active and hybrid EMI filters based on a noise model, impedance requirements, output current capability, power loss, and frequency response. First, the CM noise model for a motor drive system is studied. Active filters with both voltage and current cancellations are analyzed based on the power loss, size, and impedance requirements between the active filter and noise sources. A CM active filter with feedforward current cancellation is then proposed. Different techniques are explored for improving the performance of the proposed active filter. Hybrid filters are then investigated based on the impedance requirements between the passive filter and the active filter. The design of hybrid EMI filters is also discussed based on the frequency response of the active and the passive filters. A CM hybrid filter is finally built and tested in practical motor drive systems. The experiments show that the proposed CM active filter can achieve up to 50 dB noise attenuation at LF, a factor of 300, with low power loss. The size of the CM passive filter can be greatly reduced with the help of the developed active filter because the passive filter does not need to attenuate LF CM noise.

II. Analysis of CM EMI in a Motor Drive System

Fig. 1 shows a typical three-phase motor drive system. The power is fed to the motor drive via a dc bus. Six insulated-gate bipolar transistor (IGBT) switches drive a motor via a shielded cable. The heatsink is grounded. The noise model of motor can be represented using $C_{\rm MT}$, $C_{\rm MT2}$, $L_{\rm MT}$, and $C_{\rm G}$, where $C_{\rm G}$ is the parasitic capacitance between the windings of motor and its frame. The frame is grounded via the shield of the cable. There is CM parasitic capacitance $C_{\rm H}$ between the collectors of the IGBTs and the heatsink, and a lumped CM parasitic capacitance (not shown in the figure) between the inner conductors of the cable and its shield. Line-impedance stabilization networks (LISNs) are inserted between the motor drive and dc source for EMI measurement.

It is assumed that the electrical parameters within the three phases are symmetrical. The CM noise model of the system can be represented in Fig. 2(a). Based on the definition of CM voltage, if $V_{\rm C1}$, $V_{\rm C2}$, and $V_{\rm C3}$ are collector voltages of the three IGBT devices shown in Fig. 1, their average voltage $V_{\rm CM}$ is the CM noise source. The noise model of the cable can be represented by a transmission line. High dv/dt, which is caused by the switching of IGBT switches, charges and discharges the parasitic CM capacitance so that CM noise is generated. The CM noise flowing through the parasitic capacitance $C_{\rm H}$ is $I_{\rm CM2}$. The CM noise flowing through the parasitic capacitance $C_{\rm G}$ in the motor and the CM parasitic capacitance $3C_{\rm C}$s between the inner conductors of the cable and its shield is $I_{\rm CM1}$. $I_{\rm CM}$ is the total CM noise that flows back to the dc bus via LISNs. The CM impedance of two LISNs is $Z_{\rm LISNs}$. $Z_{\rm LISNs}$ is usually 25 Ω above 150 kHz and several ohms at 10 kHz. The equivalent circuit for CM noise is derived in Fig. 2(b) based on the Thevenin theorem.

In Fig. 2(b), $Z_{\rm CM}(s)$ is a complicated network. However, at LFs, due to the high impedance of the parasitic capacitance, $Z_{\rm CM}(s)$ is the sum of all parasitic capacitance. In experiments, the measured total CM capacitance is around 5 nF, and the impedance is much higher than the LISNs' impedance $Z_{\rm LISNs}$ below 1 MHz. In experiments, it is found that the CM noise from the motor and motor cable contributes to more than 90% of the $I_{\rm CM}$.

The original CM noise $I_{\rm CMO}(s)$ flowing through LISNs without any EMI filters inserted is given by

$$I_{\rm CMO}(s) = \frac{V_{\rm CM}(s)}{Z_{\rm CM}(s) + Z_{\rm LISNs}}. \tag{1}$$

The performance of a filter on CM noise attenuation can be evaluated by comparing the CM noise current flowing through LISNs with the filter and the original CM noise $I_{\rm CMO}(s)$.

III. Active EMI Filter for CM Noise Reduction

A. CM Noise Voltage Cancellation

In Fig. 2(a), the measured CM noise is the voltage drop of $I_{\rm CM}$ on the LISNs. If the CM noise flowing through the LISNs

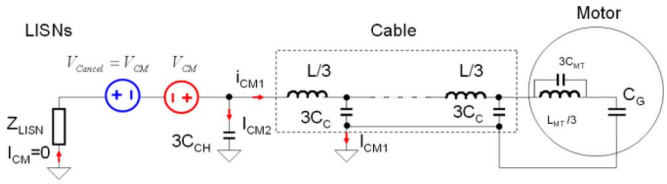

Fig. 3. CM noise voltage cancellation.

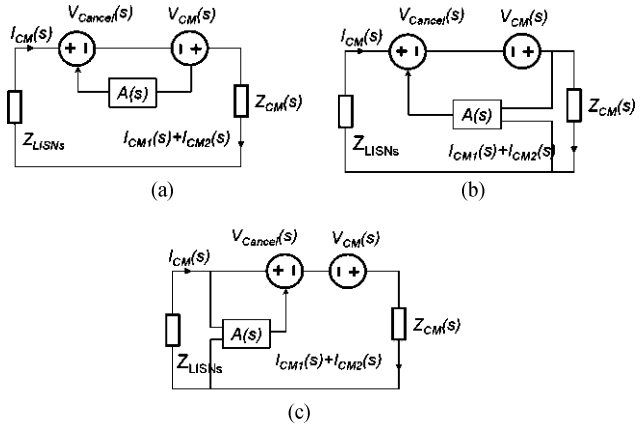

Fig. 4. CM noise voltage cancellation. (a) Feedforward. (b) Feedback 1. (c) Feedback 2.

is greatly reduced, measured CM noise would be greatly reduced. There are two possible methods for canceling CM noise. One method is to cancel the CM noise voltage $V_{\rm CM}$ in Fig. 2. Ogasawara *et al.* [5] proposes a noise voltage cancellation on the motor side to cancel the CM noise $i_{\rm CM1}$. The voltage cancellation discussed here is on the dc bus side. Fig. 3 shows the principle of this cancellation method. The benefit of this cancellation is that both the CM noise $i_{\rm CM1}$ and $i_{\rm CM2}$ can be canceled. In Fig. 3, a voltage source is generated by a cancellation circuit and is in series with CM noise source $V_{\rm CM}$. Ideally, the introduced voltage source has the same waveform as $V_{\rm CM}$, but in the opposite direction. The CM noise current in the LISNs is canceled, since the net CM noise voltage is zero.

Fig. 4 shows three approaches for CM noise voltage cancellation. Fig. 4(a) shows feedforward cancellation. Fig. 4(b) and (c) shows two feedback cancellations.

For the feedforward cancellation in Fig. 4(a), the CM noise voltage $V_{\rm CM}$ is sensed and amplified $A(s)$ times before being injected into dc bus. As stated in Section II, $V_{\rm CM}$ is the average voltage of $V_{\rm C1}$, $V_{\rm C2}$, and $V_{\rm C3}$ in Fig. 1. The dc bus is the reference potential for $V_{\rm CM}$. The CM current flowing through the LISNs is given by

$$I_{\rm CM}(s) = (1 - A(s))I_{\rm CMO}(s). \tag{2}$$

$A(s)$ should approach unity to obtain the best cancellation. For the feedback cancellation in Fig. 4(b), the CM noise voltage drop on CM noise source $Z_{\rm CM}(s)$ is sensed and amplified $A(s)$ times before being injected into the dc bus. It is worth noting that the reference potential for this sensed CM noise voltage is the ground, which is different from the feedforward case. The

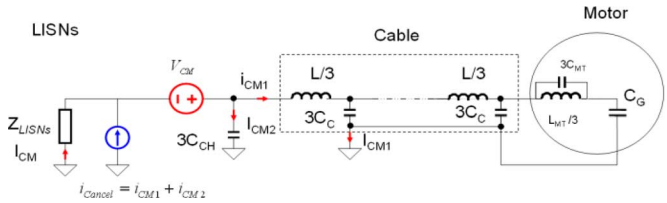

Fig. 5. CM noise current cancellation.

CM current flowing through LISNs is given by

$$I_{\rm CM}(s) = \frac{I_{\rm CMO}(s)}{1 + (A(s)/[1 + (Z_{\rm LISNs}/Z_{\rm CM}(s))])}. \tag{3}$$

Equation (3) suggests that voltage gain $A(s)$ should be high, and the feedback cancellation is more efficient if the magnitude of source impedance $Z_{\rm CM}(s)$ is not smaller than the LISNs' impedance $Z_{\rm LISNs}$

$$|Z_{\rm CM}(s)| \geq |Z_{\rm LISNs}|. \tag{4}$$

For the CM noise source, this condition can usually be met at LF since the impedance of the CM parasitic capacitance is usually very high at LF. If the same method is used for DM noise cancellation, the condition may not be met if there is a large shunt capacitor before the active filters. Thus, it is preferred to place a series inductor before this feedback active filter.

For the feedback cancellation in Fig. 4(c), the CM noise voltage drop on the LISNs is sensed and amplified $A(s)$ times before being injected into the dc bus. It should be pointed out that ground is the reference potential for this sensed CM noise voltage. The CM current flowing through LISNs is given by

$$I_{\rm CM}(s) = \frac{I_{\rm CMO}(s)}{1 + (A(s)/[1 + (Z_{\rm CM}(s)/Z_{\rm LISNs})])}. \tag{5}$$

Equation (5) shows that voltage gain $A(s)$ should be high, and the feedback cancellation is more efficient if the magnitude of source impedance $Z_{\rm CM}(s)$ is not larger than LISNs' impedance $Z_{\rm LISNs}$

$$|Z_{\rm CM}(s)| \leq |Z_{\rm LISNs}|. \tag{6}$$

For the CM noise source, this condition usually cannot be easily met at LF since the impedance of CM parasitic capacitance is usually very high at LF. If the same method is used for DM noise cancellation, the condition can be easily met if there is a large enough shunt capacitor before the active filters.

Based on these analyses of two feedback cancellation schemes, we can determine that each scheme has its own specific applications. The feedback cancellation in Fig. 4(b) is appropriate for noise with high impedance. The feedback cancellation in Fig. 4(c) is appropriate for noise with low impedance. In contrast, feedforward cancellation does not have noise impedance requirements.

B. CM Noise Current Cancellation

CM noise can also be canceled using a current source generated by a cancellation circuit, as shown in Fig. 5. In Fig. 5, a current is generated between the ground and the dc bus. Ideally,

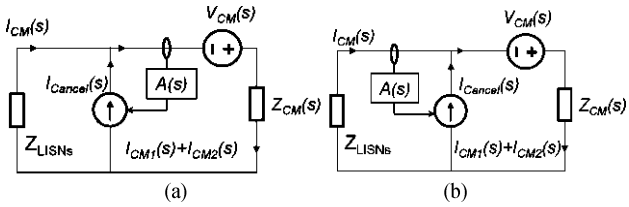

Fig. 6. CM current cancellation. (a) Feedforward. (b) Feedback.

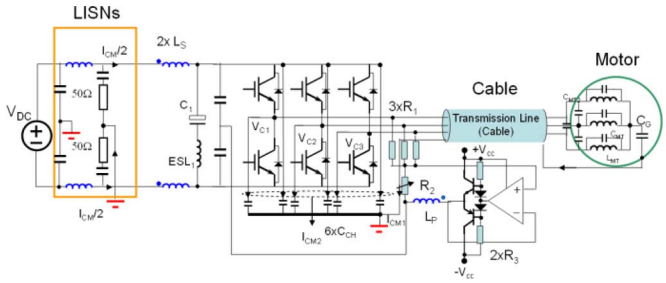

Fig. 7. Implementation of feedforward CM noise voltage cancellation.

as long as the current source has the same waveform as the CM noise current, the CM noise current flowing through the LISNs is zero. There are two implementations for CM current cancellation: feedforward cancellation and feedback cancellation. They are shown in Fig. 6(a) and (b).

In Fig. 6(a), the CM noise current is sensed on the noise source side. The sensed current is amplified $A(s)$ times and injected to the dc bus with reference to the ground. The CM noise current flowing through the LISNs is given by

$$I_{\mathrm{CM}}(s) = \frac{1 - A(s)}{1 - A(s)/\left(1 + [Z_{\mathrm{CM}}(s)/Z_{\mathrm{LISNs}}]\right)} I_{\mathrm{CMO}}(s). \quad (7)$$

Equation (7) shows that current gain $A(s)$ should approach unity, and the feedforward cancellation is more efficient if the magnitude of source impedance $Z_{\mathrm{CM}}(s)$ is not smaller than LISNs' impedance Z_{LISNs}

$$|Z_{\mathrm{CM}}(s)| \geq |Z_{\mathrm{LISNs}}|. \quad (8)$$

For a CM noise source, this condition can usually be met at LF since the impedance of CM parasitic capacitance is usually very high at LF. If the same method is used for DM noise cancellation, the condition may not be met if there is a large shunt capacitor before the active filters. It is, therefore, preferred to place a series inductor before active filters using feedforward current cancellation.

The feedforward cancellation demands only a unity current gain for current amplifier. It is easier to achieve a wider bandwidth than feedback cancellation; therefore, feedforward cancellation is used in the experiments performed for this paper.

In Fig. 6(b), the CM noise current is sensed on the LISNs' side. The sensed current is amplified $A(s)$ times and injected to the dc bus from the ground. The CM noise current flowing through LISNs is given by

$$I_{\mathrm{CM}}(s) = \frac{I_{\mathrm{CMO}}(s)}{1 + [A(s)/\left(1 + [Z_{\mathrm{LISNs}}/Z_{\mathrm{CM}}(s)]\right)]}. \quad (9)$$

Equation (9) shows that current gain $A(s)$ should be high, and this feedback cancellation is more efficient if the magnitude of source impedance $Z_{\mathrm{CM}}(s)$ is not smaller than the LISNs' impedance Z_{LISNs}

$$|Z_{\mathrm{CM}}(s)| \geq |Z_{\mathrm{LISNs}}|. \quad (10)$$

For a CM noise source, this condition can usually be met at LF since the impedance of the CM parasitic capacitance is usually very high at LF. If the same method is used for DM noise cancellation, the condition may not be met if there is a large shunt capacitor before the active filters. Therefore, it is preferred to have a series inductor before the active filters using feedback current cancellation. The feedback cancellation demands a high current gain for the current amplifier to achieve cancellation. Since the gain bandwidth of the amplifier is limited, the bandwidth of the current cancellation would be not as high as that of feedforward cancellation.

C. Implementations of CM Active Filter

The proposed implementation for feedforward noise voltage cancellation is shown in Fig. 7. In Fig. 7, a voltage divider senses the CM noise voltage between the neutral point and the dc bus. The voltage divider is composed of three R_1s and one R_2. R_2 can be adjusted to compensate any mismatched voltage gain in the cancellation. The voltage amplifier, including the voltage divider and the transformer, has a unit gain. The cancellation belongs to the type of feedforward cancellation shown in Fig. 4(a). In contrast, if the sensed noise voltage is between the neutral and the ground, the cancellation would belong to the feedback cancellation method shown in Fig. 4(b). In that case, the gain of the voltage amplifier should be high.

In Fig. 7, the voltage between the neutral point and the dc bus is sensed and fed to the input of a class-AB amplifier. A class-AB amplifier is a good tradeoff between efficiency, linearity, and speed. The amplifier is a voltage follower with a high-current-driving capability. The amplifier drives the primary winding of a transformer (L_P). The secondary winding of the transformer (L_S) is in series with the dc bus. By designing the ratio of the voltage divider and the turn ratio of the transformer, a voltage with the same waveform as the CM noise voltage can be injected. The coupling polarity of the primary and the secondary windings should be designed to guarantee the voltage cancellation, as shown in the figure.

In Fig. 7, the power supply voltage V_{CC} of the cancellation circuit is much lower than bus voltage V_{DC}. The output of the voltage divider should be lower than V_{CC} to guarantee the normal operation of the amplifier. The turn ratio of the transformer should compensate the voltage ratio of the voltage divider so that the voltage gain of the cancellation circuit is equal to one. This relationship can be represented using primary inductance L_P and secondary inductance L_S as

$$\frac{L_P}{L_S} = \left(\frac{3R_2}{R_1 + 3R_2}\right)^2. \quad (11)$$

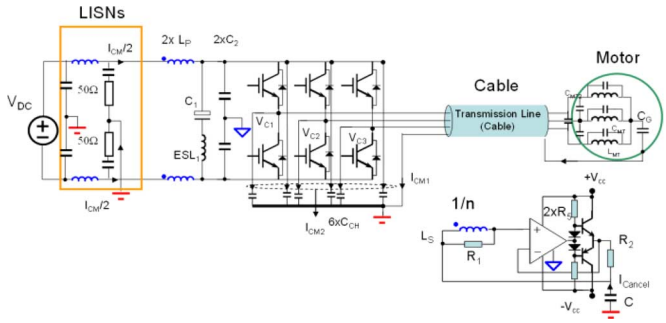

Fig. 8. Implementation of feedback CM noise current cancellation.

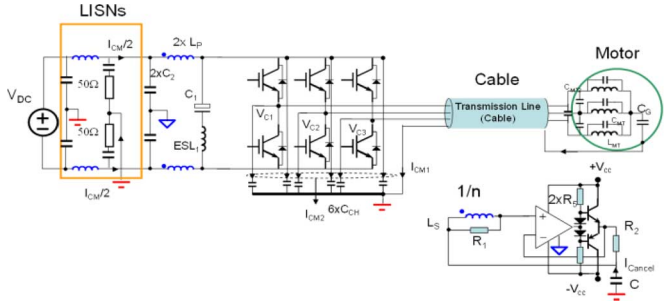

Fig. 9. Implementation of feedforward CM noise current cancellation.

One of the advantages for the implementation in Fig. 7 is that widely available low-voltage-rating transistors and operational amplifiers can be used. However, there is a disadvantage to this implementation. The transformer's primary inductance cannot be small, since small inductance leads to high magnetizing current, and thus, high power loss on two transistors. Because the high turn ratio of the transformer is needed to compensate the voltage ratio of the voltage divider, the inductance of the secondary winding is large. At the same time, the secondary winding carries a full load current, so the cross-sectional area of the winding is not small. As a result, the size of the transformer would not be small. This contradicts the purpose of reducing the size of EMI filters using active filters. Because of this, the disadvantages of voltage cancellation are high power loss and a large transformer size.

The CM current cancellations can be implemented, as shown in Figs. 8 and 9. This paper proposes a current-controlled current source to inject cancellation current between the dc bus and the ground. The advantage of the proposed current source is that the injecting point is toward the ground, so that an isolation capacitor (C) can be used to isolate the active EMI filter from the ground. Fig. 8 shows the feedback implementation and Fig. 9 shows the feedforward implementation.

In Fig. 8, a current transformer is used to sense CM noise current on the dc bus. The transformer's primary winding has only one turn. If the secondary winding has n turns, the turn ratio of the current transformer would be $1/n$. The current transformer's size is much smaller than that of the voltage transformer for the voltage cancellation in Fig. 7. The sensed current has a voltage drop on R_1. The voltage drop is fed to the input of an amplifier. The output current of the amplifier is sensed on R_2. The sensed

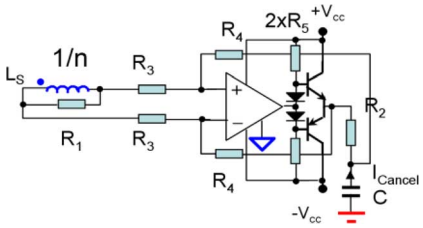

Fig. 10. Current-controled current source used as an active filter.

signal is fed back to the input loop to be compared with the sensed current on R_1. The current gain of the active filter is given by (12). The cancellation current is injected to the ground via injection capacitor C. It should be noted that the power ground of the amplifier is connected to the center tap of two series C_2s on the dc bus. The injected cancellation current can therefore freely flow in the loop composed of the active filter, ground, LISNs, and dc bus. The injection is between the center tap of two C_2s and the ground. The injection point is on the noise side, and the current-sensing point is on the LISNs side, so the implementation in Fig. 8 is a feedback cancellation. The proposed active filter in Fig. 8 is a current-controlled current source, which is different from the open-loop current sources proposed in some papers

$$A = \frac{R_1}{nR_2}. \tag{12}$$

In Fig. 9, the current is injected on the LISNs side and the current-sensing point is on the noise side, and therefore, it is a feedforward cancellation. As discussed previously, the gain of the active filter should be equal to one, and therefore, the condition in (13) should be met

$$n = \frac{R_1}{R_2}. \tag{13}$$

The more flexible current-controlled current source that is finally proposed and used in experiments is shown in Fig. 10. In Fig. 10, for feedback implementation, the gain of the current source is given by (14). For feedforward implementation, the condition for unit gain is given by (15). Here, again, n is the turn ratio of the current transformer

$$A = \frac{R_1 R_4}{nR_3}\left(\frac{1}{R_2} + \frac{1}{2R_4}\right) \approx \frac{R_1 R_4}{nR_3 R_2} \tag{14}$$

$$n = \frac{R_1 R_4}{R_3}\left(\frac{1}{R_2} + \frac{1}{2R_4}\right) \approx \frac{R_1 R_4}{R_3 R_2}. \tag{15}$$

It should be noted that the neutral voltage will be rebuilt with reduced amplitude on injection capacitor C. This is because CM noise is generated when the neutral voltage charges and discharges CM parasitic capacitance. On the other hand, the current source, which has the same waveform as the CM noise current, charges and discharges the injection capacitor C. It is a reverse process, so the neutral voltage is rebuilt on injection capacitor C with reduced amplitude. As a result, the value of C should meet the condition given in (16) to guarantee the output of the current source is not saturated by the limited power supply

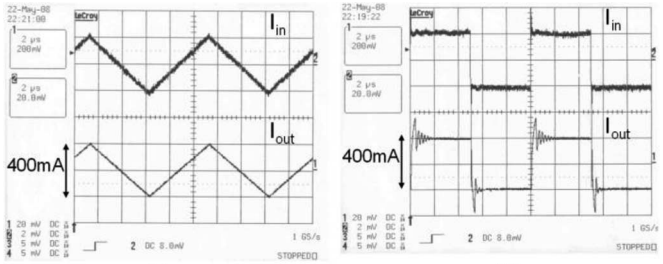

Fig. 11. Response of the developed active EMI filter. (a) Triangular-wave response. (b) Square-wave response.

voltage $V_{\rm CC}$

$$C > \frac{V_{\rm dc}}{2V_{\rm CC}} \sum C_{\rm CM}. \tag{16}$$

The value $\sum C_{\rm CM}$ in the aforementioned equation is the total CM parasitic capacitance, which includes the parasitic capacitance in the motor drive, cable, and motor.

Active EMI filters can be directly used to reduce EMI noise when the noise is relatively low so that no significant power loss is introduced by active filters. When the noise is high, passive EMI filters should be introduced before the active filters to reduce the noise. EMI filters, including both passive and active filters, are called hybrid EMI filters. Furthermore, due to the limitations of slew rate, phase shift, and gain bandwidth, active EMI filters are supposed to suppress noise at relatively LFs.

IV. Experiments on Active Filters

This section describes the experimental implementation of the current-controlled current-source active filter shown in Fig. 10. The current transformer is made using a ferrite toroidal core. For a good current transformer design, the reflected resistance from the secondary side to the primary side should be much smaller than the impedance of the magnetizing inductance of the primary winding, so that the magnetizing inductance would not affect the current sensing. This condition is given by (17). In experiments, W material with a relative permeability of 10 000 from Magnetics Company is used for the core. The core's model number is 42507TC. The winding has 100 turns and is made using wire AWG 34

$$\frac{R_1}{n^2} \ll |j\omega L_P|. \tag{17}$$

The inductance L_P is around 8 μH, which corresponds to an impedance of 502 mΩ at 10 kHz. On the other hand, the reflected resistance is around 1.152 mΩ (R_1 is 10 Ω and resistance of the secondary winding is 1.52 Ω). The condition in (17) is met. The resistance of the secondary winding should be much smaller than $R1$ to reduce its effects on current sensing. However, its effects can be compensated by adjusting the gain of the amplifier. The isolation capacitor has a capacitance of 100 nF in experiments.

The active filter is measured using a signal generator and an oscilloscope. The measurement results are shown in Fig. 11. The peak–peak value for the waveforms in Fig. 11 is 400 mA, and the frequency is 100 kHz. The top waveforms are excitations and the bottom waveforms are output currents. Fig. 11(a) shows the triangular-wave response, and Fig. 11(b) shows the square-wave response. The triangular-wave response is pretty good, but there is ringing observed on square-wave responses at the rising and falling edges.

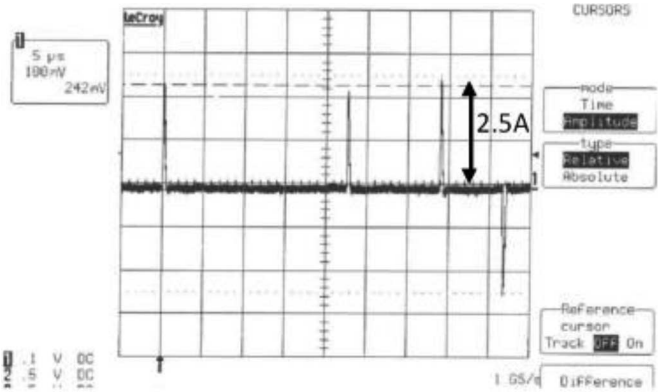

Fig. 12. Waveform of the original CM noise current.

The active filter is then tested in a motor drive system. In experiments, a 2.5-kW motor drive system with a switching frequency of 12 kHz is tested. The CM noise current waveform is first measured without any EMI filters inserted. The measured waveform is shown in Fig. 12. The CM noise spikes have an amplitude of 2.5 A with a slope of 7.2×10^6 A/s. The experiments show that the active filter cannot accurately follow such a high amplitude and high di/dt current. This verifies that active EMI filters are not good at suppressing high di/dt and high-amplitude CM noise spikes. Therefore, using a small passive EMI filter before an active filter to reduce the amplitude and di/dt of the CM current is a good approach.

V. Improvement of Active Filter Performance

To maximize the benefits of the active filter on the reduction of the passive filter size, the active filter's performance must be optimized before it can be integrated with a passive filter. Its performance can be improved in terms of the following four aspects: increasing output current capability, eliminating HF ringing, reducing power loss, and fine-tuning cancellation gain.

A. Increase Output Current Capability

With increased output current capability, the active filter can suppress higher noise than those with smaller current capabilities. It may, therefore, be solely used to suppress LF noise so that a passive filter will handle HF noise only. The size of a passive EMI filter would be reduced since its corner frequency is greatly increased.

In order to increase output current capability, the limitation of the output current is analyzed in Fig. 13 and

$$I_{\rm cancelMax} = \beta I_{\rm BMax} \tag{18}$$

$$I_{\rm BMax} \le \frac{2(V_{\rm CC} - V_{\rm p\text{-}n})}{R_5}. \tag{19}$$

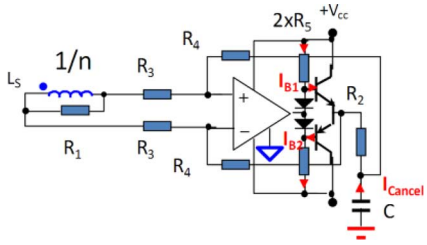

Fig. 13. Analysis of the output current capability of the developed active filter.

In Fig. 13, the maximum output current $I_{\mathrm{cancelMax}}$ of the active filter is determined by the current gain β and the maximum base current I_{BMax} of the transistors, as shown in (18). At the same time, the I_{Bmax} is determined by the maximum bias current shown in (19). In (19), V_{CC} is the power supply voltage and $V_{\mathrm{p\text{-}n}}$ is the voltage drop of the diode p-n junction. From (19), in order to increase the current capability, R_5 should be reduced. In experiments, when two R_5s are reduced 3.2 times, the output current capability increases by around three times. To keep two transistors in class-AB mode, the voltage drops of the bias diodes should not increase when the two R_5s are reduced. In order to achieve this, higher current-rating diodes can be used, or alternatively, more diodes can be paralleled.

B. Reduce Power Loss

The power stage consumes most of power of the active filter, although it works in class-AB mode. Low power loss would benefit the system efficiency and power density.

It should be noted that the cancellation current I_{cancel} itself would not generate power loss on isolation capacitor C since it is a reactive component. Furthermore, in Fig. 6(a), after the CM noise is canceled, $I_{\mathrm{CM}}(s)$ is zero, so the noise voltage drop on the LISNs side is zero. This means, ideally, I_{cancel} would not cause any extra power loss outside of the active filter. The only power loss comes from the active filter itself.

Based on circuit theory, it can be derived that, for an ideal class-AB amplifier with the capacitor load shown in Fig. 10, if the output is not saturated, the power loss of two transistors is

$$P_{\mathrm{loss}} = V_{\mathrm{CC}} \overline{I}_{\mathrm{cancel}} \tag{20}$$

where $\overline{I}_{\mathrm{cancel}}$ is the average of the absolute value of cancellation current.

The actual loss may be a little bit higher, depending on the bias current. There are also other power losses caused by components like the operational amplifier and the bias circuit. However, the power loss from the two transistors is dominant when the noise current is higher than the sum of the bias current and the current drawn by the operational amplifier. The power loss in (20) is proportional to the product of the average cancellation current and power supply voltage V_{CC}. Since the cancellation current is the same as the noise current, only the power supply voltage can be reduced to reduce power loss. The minimum V_{CC} is the voltage at which the output is on the boundary of being saturated. It is equal to the maximum voltage on isolation capacitor C plus V_{be}, the voltage drop between base and emitter,

TABLE I
MEASURED POWER LOSS OF AN ACTIVE FILTER

±VCC	$\overline{I}_{cancel}$ @ 100kHz (Sinusoidal wave)	P_{loss}
±15V	128mA	2.34W
	64mA	1.32W
±8V	128mA	1.20W
	64mA	640mW
±5V	128mA	750mW
	64mA	390mW

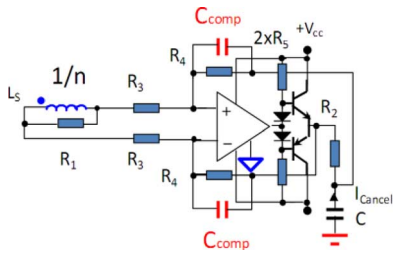

Fig. 14. Eliminate the ringing using compensation.

of the transistors. As stated before, the voltage on the isolation capacitor is the integration of I_{cancel} on isolation capacitor C. Either a small I_{cancel} or a large capacitance C can lead to small voltages on isolation capacitor C, which leads to a small V_{CC} and small power loss. Different applications may have different requirements for the largest capacitance between the dc bus and the ground. However, it should be mentioned that the behavior of isolation capacitor C in this active filter is different from that of a directly grounded capacitor, since its current is controlled by the active filter instead of the voltage between the bus and the ground. Thus, even if this active filter works for an ac bus, the isolation capacitor would not generate leakage current as a directly grounded capacitor does.

Table I shows a measured power loss of the active filter with different values for V_{CC} and $\overline{I}_{\mathrm{cancel}}$. The power loss is proportional to the product of noise current $\overline{I}_{\mathrm{cancel}}$ and V_{CC}, which verifies the analysis mentioned previously.

Based on the aforementioned analysis, the power loss can be reduced by reducing V_{CC} as long as the output is not saturated. In a practical application, depending on the noise level, V_{CC} can be adapted to a certain level to minimize the power loss and at the same time keep the active filter working properly.

C. Phase Compensation to Eliminate HF Ringing

Due to the insufficient phase margin in the active filter, a 3.3-MHz ringing is observed in the square-wave response test shown in Fig. 11(b). This ringing will be injected to the system; as a result, there will be a noise peak at 3.3 MHz. The gain or phase of the active filter must be compensated to eliminate this ringing. A phase-lead compensation is introduced by simply paralleling two compensation capacitors C_{comp}s with two R_4s, as shown in Fig. 14. C_{comp} and R_4 introduce a corner frequency at 2.1 MHz. This leads to a more than 50° phase margin, which eliminates the ringing at 3.3 MHz. The compensation capacitor cannot be too large; otherwise, the active filter's bandwidth could be limited.

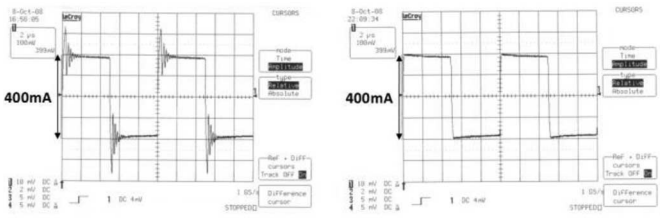

Fig. 15. Ringing is eliminated with compensation. (a) Before compensation. (b) After compensation.

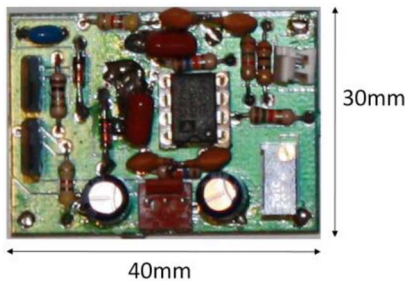

Fig. 16. Prototype of the developed active filter.

The comparison of square-wave responses before and after compensation is shown in Fig. 15. This figures shows that the ringing is eliminated after compensation.

D. Fine-Tuning Gain for Better CM Noise Cancellation

Equation (15) describes the design of an active filter with feedforward current cancellation. In a practical design, all resistors have tolerance; furthermore, the secondary winding of current transformer has resistance, which may not be ignored when comparing to 10 Ω resistance of R_1. Because of these, the gain of an active filter would not be exactly equal to one; therefore, it cannot achieve the best cancellation. If the resistor tolerance and winding resistance can be compensated by adjusting the resistance of R_1, R_3, or R_4, the cancellation can be improved. In experiments, the resistor R_3 is finally adjusted to achieve better cancellation.

Fig. 16 shows the prototype of the active filter. Its size would be even smaller if surface mount components were used.

VI. Hybrid CM EMI Filter Design

As discussed in Section IV, passive filters should be used before active filters to reduce the amplitude and the di/dt of the CM current so that the active filters can work properly. For the typical CM noise current shown in Fig. 12, Fourier analysis shows that the amplitude of LF harmonics is much smaller than the amplitude of the CM noise current. If a passive filter can attenuate the HF noise, the active filter can easily handle the LF noise. This concept can be described using insertion loss in the frequency domain in Fig. 17.

In Fig. 17, the active filter attenuates LF noise, and the passive filter attenuates the HF noise. In the middle frequency range, both the active and passive filters attenuate noise. Because the passive filter does not need to attenuate LF noise, its corner frequency can be greatly increased. As a result, the passive filter's size is significantly reduced.

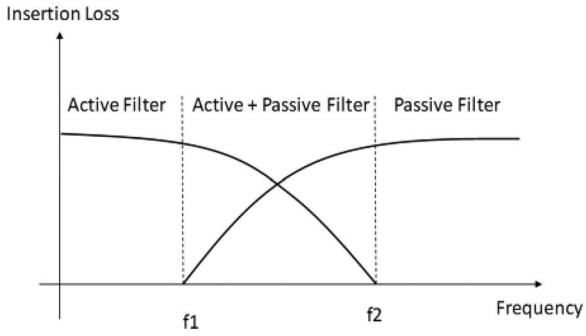

Fig. 17. Insertion loss of the active and passive filters in a hybrid EMI filter.

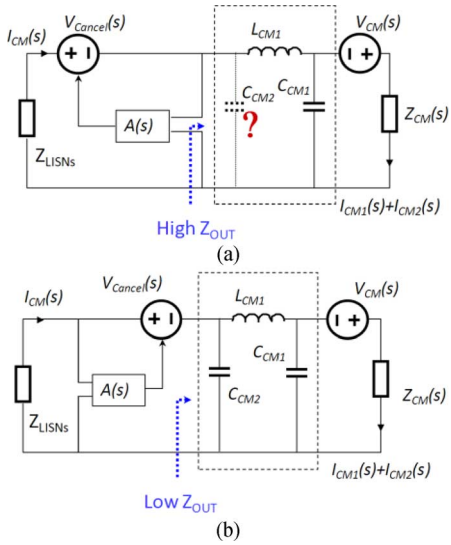

Fig. 18. Hybrid EMI filters with voltage cancellation. (a) Feedback 1. (b) Feedback 2.

The principle of the impedance requirement discussed in Section III still applies to hybrid EMI filters. As discussed in Section III, different active EMI filters have different requirements for impedance. Because of this, hybrid EMI filters should be analyzed based on the impedance relationship between active filters and passive filters. Two cases are analyzed here. For the first case, there is a passive filter in the first stage and an active filter in the second stage. For the second case, there is a passive filter in the first stage and a passive filter in the third stage. An active filter is in the second stage. Based on the impedance requirements derived in Section III, Figs. 18–21 show some possible structures for hybrid EMI filters. For voltage cancellations, two feedback methods are analyzed. For current cancellations, both feedforward and feedback are analyzed.

For the feedback voltage cancellation shown in Fig. 18(a), the active filter requires high output impedance from the passive filter. If the impedance of C_{CM2} is smaller than the impedance Z_{LISNs} within the interested frequency range, C_{CM2} would not be preferred, since it degrades the performance of the active filter. In this case, series inductor L_{CM1} would be preferred

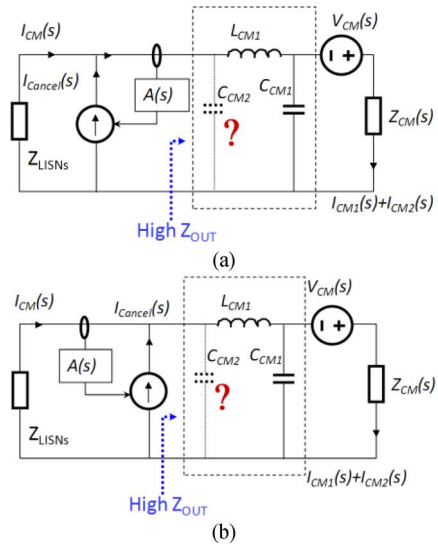

Fig. 19. Hybrid EMI filters with current cancellation. (a) Feedforward. (b) Feedback.

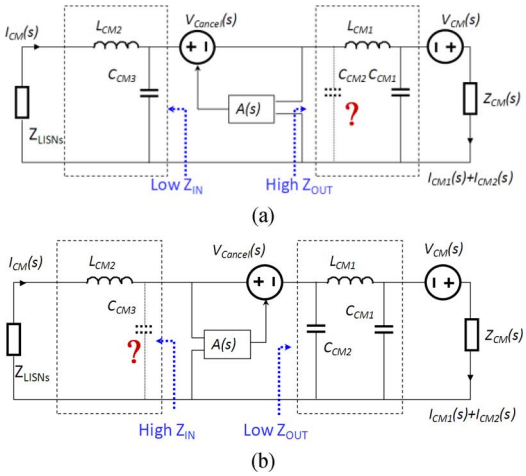

Fig. 20. Hybrid EMI filters with voltage cancellation. (a) Feedback 1. (b) Feedback 2.

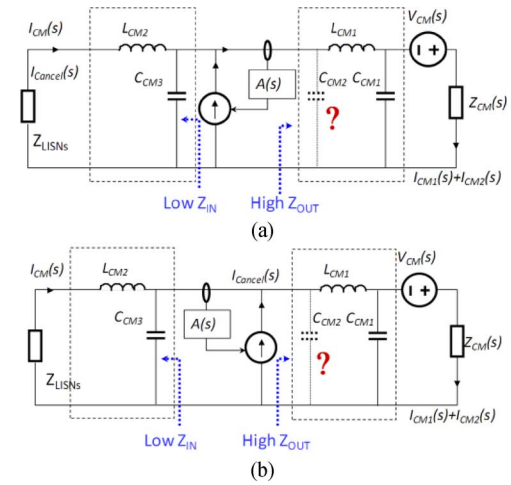

Fig. 21. Hybrid EMI filters with current cancellation. (a) Feedforward. (b) Feedback.

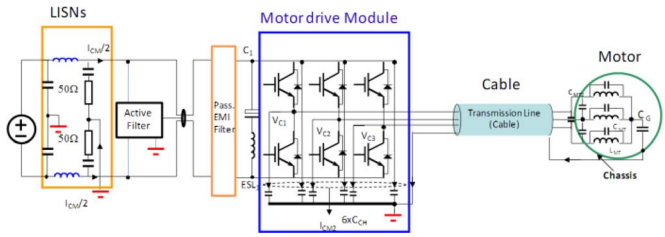

Fig. 22. Developed hybrid EMI filter used in a motor drive system.

because it helps to increase the output impedance of the passive filter.

For the feedback voltage cancellation shown in Fig. 18(b), the active filter requires low impedance from the passive filter. The shunt capacitor $C_{\rm CM2}$ would be preferred since it helps reduce the output impedance of the passive filter.

In Fig. 19, both feedforward and feedback current cancellations require high output impedance from the passive filter. For the same reason as in Fig. 18, shunt capacitor $C_{\rm CM2}$ would not be preferred if its impedance is smaller than the impedance $Z_{\rm LISNs}$ within the interested frequency range. Series inductor $L_{\rm CM1}$ is preferred since it helps increase the output impedance of the passive filter.

Figs. 20 and 21 show a different structure of hybrid filters. The first and the third stages are passive filters, and the second stage is an active filter. For the feedback voltage cancellation in Fig. 20(a), the output impedance of the passive filter in the first stage should be larger than the input impedance of the passive filter in the third stage. For the feedback voltage cancellation in Fig. 20(b), the output impedance of the passive filter in the first stage should be smaller than the input impedance of the passive filter in the third stage. The shunt capacitors $C_{\rm CM2}$ in Fig. 20(a) and $C_{\rm CM3}$ in Fig. 20(b) would not be preferred if their impedances could not meet these impedance conditions.

For the feedforward current cancellation in Fig. 21(a) and the feedback current cancellation in Fig. 21(b), the output impedance of the passive filter in the first stage should be larger than the input impedance of the passive filter in the third stage. The shunt capacitor $C_{\rm CM2}$ would not be preferred if its impedance were not higher than the input impedance of the passive filter in the third stage.

Active filters help to increase the corner frequencies of passive filters, which results in a smaller filter size. If the size reduction of the passive filters is more than the size increase due to the active filters, the total size of the hybrid EMI filters would be reduced. Since most of the components in the active EMI filters can be easily integrated into an IC or with IGBT modules, the size increase would be small. As a result, it is possible to reduce the total size of the hybrid filters.

Fig. 22 shows an application of a hybrid EMI filter in a 2.5-kW motor drive system with a switching frequency of 12 kHz and a 300 $V_{\rm dc}$ bus. The feedforward current cancellation active filter developed in Sections III–V is used in the hybrid filter. In Fig. 23, a one-stage passive EMI filter is used before the active filter. The filter inductor uses three nanocrystalline cores in parallel. The nanocrystalline core is FT-3KM

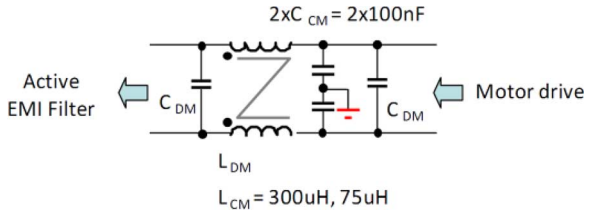

Fig. 23. Passive EMI filter used in the hybrid EMI filter.

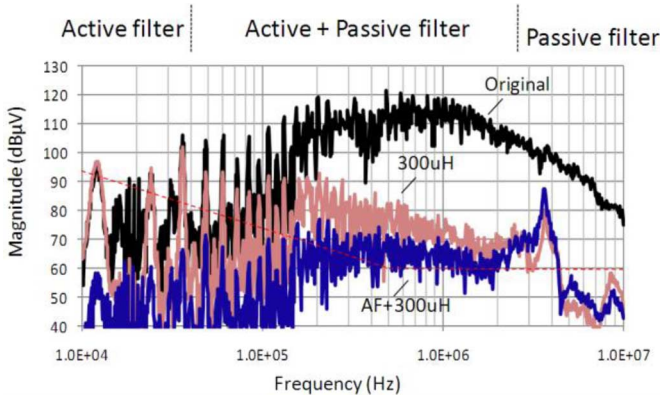

Fig. 24. Comparison of the measured CM noise.

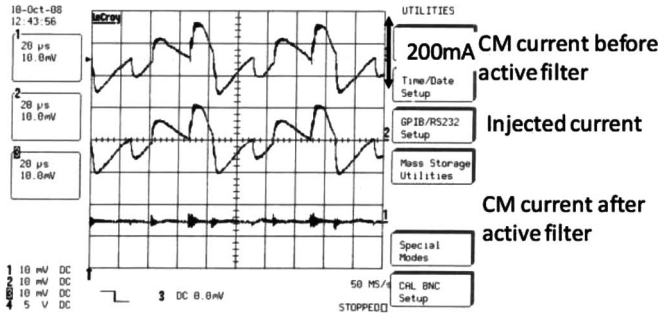

Fig. 25. Comparison of the measured current in time domain.

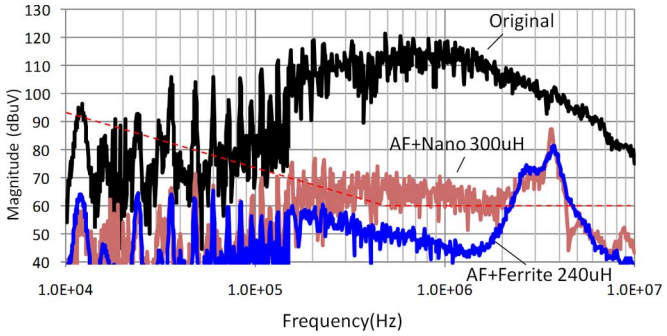

Fig. 26. Effects of magnetic material on hybrid filters: nanocrystalline versus ferrite.

K1208 A from Metglas, Inc. At LFs, nanocrystalline has higher permeability and saturation flux density than ferrite, and therefore, the size of a nanocrystalline inductor is smaller than that of a ferrite inductor. All CM component values are shown in the figure. As stated in Section II, at LFs, the CM source impedance of the motor drive is a parasitic capacitance C_S (5 nF). The output impedance of the CM filter is therefore

$$|Z_{\rm OUT}| = \left| j\left[\omega L_{\rm CM} - \frac{1}{\omega(2C_{\rm CM} + C_S)}\right] + R_{\rm loss} \right| \qquad (21)$$

where $R_{\rm loss}$ is the equivalent resistance for the power loss in the inductor, capacitor, and the CM noise path. Because $Z_{\rm LISNs}$ is only several ohms at 12 kHz, the output impedance of the passive filter meets the condition in (8).

The EMI measurement is carried out with the same setup as that used in Fig. 22. The CM noise is measured with the help of a noise separator [13]. The CM noise is first measured without any filters applied. In the second step, the passive EMI filter, which has a 300-μH CM inductance, is inserted into the dc bus between the motor drive and LISNs. The CM noise is measured. In the third step, the feedforward current cancellation active filter developed in Sections IV and V is connected between the passive filter and LISNs. The CM noise is measured. The measured CM noise of each step is compared in Fig. 24.

Fig. 24 shows that noise attenuation below 40 kHz is achieved only by an active filter. Noise attenuation between 40 kHz and 2.5 MHz is achieved by both active and passive filters. Noise attenuation above 2.5 MHz is achieved by the passive filter only. This is same as described in Fig. 17. At 12 and 36 kHz, a 39-dB attenuation is achieved by the active filter. As a comparison, if there is no active filter applied, the passive filter needs to have an 85.8-mH CM inductor to achieve the same attenuation at 12 kHz. The size of an 85.6-mH inductor would be much larger than the size of a 300-μH inductor; therefore, by using a hybrid filter, it is possible to reduce the filter's total size.

Time domain waveforms are also measured and compared in Fig. 25. In Fig. 25, three waveforms are compared. The first waveform is the CM noise current after the passive filter. The second waveform is the injected cancellation current. The third waveform is the CM current after the hybrid filter. Fig. 25 shows that the cancellation current can accurately follow the CM current, so that the CM noise is greatly reduced.

In the experiments, the active filter works for either ± 8 or ± 15 V $V_{\rm CC}$. The power loss of the active filter is around 1 W for ± 8 V and 2 W for ± 15 V. Compared with a 2.5-kW system power, it is negligible. The power loss can be further reduced by increasing the capacitance of the isolation capacitor. For example, if the capacitance is increased by two times, the ± 5 V can be used for $V_{\rm CC}$; the power loss can thus be reduced to 0.7 W.

The EMI standard MIL-STD-461E is also shown in Fig. 24. In the middle frequency range, the CM noise is higher than the limit line. Further investigation disclosed that the permeability of nanocrystalline drops very fast as frequency increases. This leads to a lower inductance than a ferrite core in the middle frequency range. Fig. 26 shows the comparison between nanocrystalline core and ferrite core. Although ferrite inductor has a smaller inductance than nanocrystalline inductor (240 versus 300 μH) at 12 kHz, it has a better performance in the

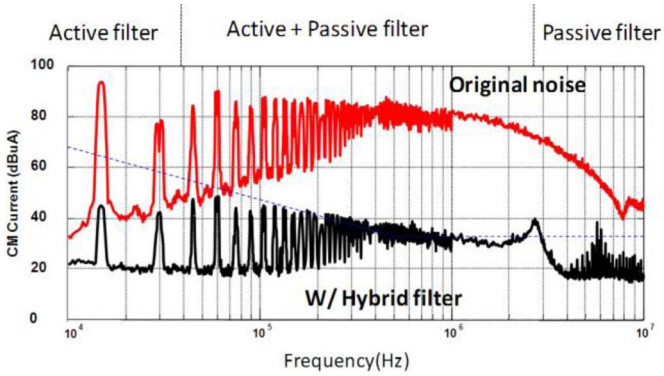

Fig. 27. Comparison of the measured CM noise.

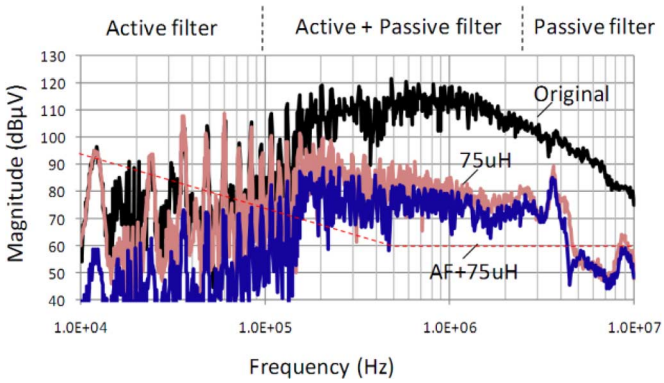

Fig. 28. Comparison of the measured CM noise.

middle frequency range because the permeability of nanocrystalline drops too much. The purpose of the measurement here is to verify the principle discussed in this paper. In order to adapt the filter to certain applications, the passive filter used here should be further improved. A hybrid magnetic material approach has been investigated recently to include the benefits of both nanocrystalline and ferrite, but it is out of the scope of this paper.

The hybrid filter prototype with the nanocrystalline core is further tested in the project sponsor's EMI laboratory. Fig. 27 shows the measured CM noise current with and without the hybrid filter. Around 50 dB, attenuation of a factor of 300 is achieved by the active filter at the first noise peak, as shown in Fig. 27.

In the last experiment, the CM inductance in the passive filter is reduced to 75 μH (nanocrystalline core). The CM noise with the passive filter and with the hybrid filter is measured and compared with the original noise in Fig. 28.

Fig. 28 shows that the noise attenuation below 100 kHz is almost achieved by just the active filter. Noise attenuation between 100 kHz and 3 MHz is achieved by both the active and passive filters. Noise attenuation above 3 MHz is achieved by the passive filter only. The active filter achieves 38 dB attenuation at 12 kHz. On the other hand, the passive filter plays a major role above 200 kHz. Once again, the nanocrystalline inductor

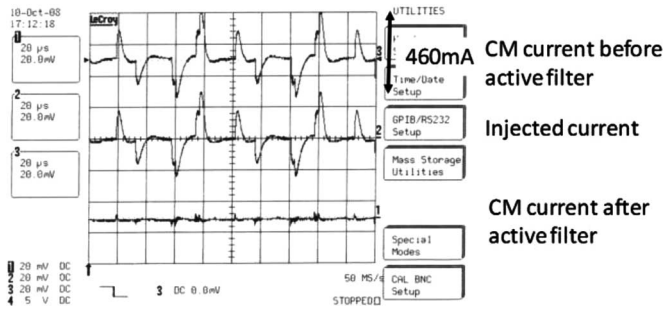

Fig. 29. Comparison of the measured current in time domain.

does not perform well in the middle frequency range since its permeability drops fast as frequency increases.

The measured time-domain waveforms are shown in Fig. 29. The active filter can properly follow the CM noise, so the CM noise after the hybrid filter is greatly reduced.

In this section, after first investigating hybrid filters based on the frequency response of the active and the passive filters, the impedance requirement between the passive and active filters, and the structures of the passive filters, a hybrid filter, which includes the active filter developed in Sections IV and V and a passive filter, is built and tested in practical motor drive systems. Experimental results show that the proposed hybrid filter can achieve good performance from LF to HF. The inductance of the passive filter can be greatly reduced because the active filter can greatly reduce the LF noise. As discussed in previous sections, most of the components in the active filter can be integrated into an IC or with the main motor drive circuit, so that the CM EMI filter's size could be greatly reduced.

The analysis of the active filter in this paper can be applied to any motor drive systems with different dc sources. When the dc source is a three-phase ac/dc rectifier, attention should be paid to the design of the HF passive filter so that it would not be saturated by the LF CM current generated by the ac/dc rectifier.

VII. Conclusion

In this paper, the CM noise model of a motor drive system was first investigated. Based on the developed CM noise model, both CM voltage and CM current cancellations were analyzed. The impedance requirements of the noise source, load, and active EMI filters were investigated. A high-performance active filter was proposed and optimized from output current capability, power loss, phase compensation, and the accurate gain of the active filter. The impedance requirements between the active filter and the passive filter in a hybrid filter also was investigated. A high-performance hybrid filter was finally built and tested in motor drive systems. The testing results verified the theoretical analysis and the design of the active and hybrid filters proposed in this paper.

References

[1] S. Wang, F. C. Lee, D. Y. Chen, and W. G. Odendaal, "Effects of parasitic parameters on EMI filter performance," *IEEE Trans. Power Electron.*, vol. 19, no. 3, pp. 869–877, May 2004.

[2] S. Wang, F. C. Lee, and W. G. Odendaal, "Characterization and parasitic extraction of EMI filters using scattering parameters," *IEEE Trans. Power Electron.*, vol. 20, no. 2, pp. 502–510, Mar. 2005.
[3] S. Wang, R. Chen, J. D. van Wyk, F. C. Lee, and W. G. Odendaal, "Developing parasitic cancellation technologies to improve EMI filter performance for switching mode power supplies," *IEEE Trans. Electromagn. Compat.*, vol. 47, no. 4, pp. 921–929, Nov. 2005.
[4] X. Chen, D. Xu, F. Liu, and J. Zhang, "Novel inverter-output passive filter for reducing both differential- and common-mode dv/dt at the motor terminals in PWM drive systems," *IEEE Trans. Ind. Electron.*, vol. 54, no. 1, pp. 419–426, Feb. 2007.
[5] S. Ogasawara, H. Ayano, and H. Akagi, "An active circuit for cancellation of common-mode voltage generated by a PWM inverter," *IEEE Trans. Power Electron.*, vol. 13, no. 5, pp. 835–841, Sep. 1998.
[6] A. L. Julian, G. Oriti, and T. A. Lipo, "Elimination of common-mode voltage in three-phase sinusoidal power converters," *IEEE Trans. Power Electron.*, vol. 14, no. 5, pp. 982–989, Sep. 1999.
[7] W. C. Ho, C. K. Lee, X. Liu, P. K. W. Chan, S. Y. R. Hui, and Y. S. Lee, "A hybrid EMI filter with ultra-wide bandwidth," in *Proc. IEEE Appl. Power Electron. Conf.*, Feb. 24–28, 2008, pp. 676–681.
[8] T. Farkas and M. F. Schlecht, "Viability of active EMI filters for utility applications," *IEEE Trans. Power Electron.*, vol. 9, no. 3, pp. 328–336, May 1994.
[9] D. C. Hamili, "An efficient active ripple filter for use in DC-DC conversion," *IEEE Trans. Aerosp. Electron. Syst.*, vol. 32, no. 3, pp. 1077–1084, Jul. 1996.
[10] N. K. Poon, J. C. P. Liu, C. K. Tse, and M. H. Pong, "Techniques for input ripple current cancellation: classification and implementation," *IEEE Trans. Power Electron.*, vol. 15, no. 6, pp. 1144–1152, Nov. 2000.
[11] M. Zhu, D. J. Perreault, V. Caliskan, T. C. Neugebauer, S. Guttowski, and J. G. Kassakian, "Design and evaluation of feedforward active ripple filters," *IEEE Trans. Power Electron.*, vol. 20, no. 2, pp. 276–285, Mar. 2005.
[12] A. C. Chow and D. J. Perreault, "Design and evaluation of a hybrid passive/active ripple filter with voltage injection," *IEEE Trans. Aerosp. Electron. Syst.*, vol. 39, no. 2, pp. 471–480, Apr. 2003.
[13] S. Wang, F. C. Lee, and W. G. Odendaal, "Characterization, evaluation and design of noise separator for conducted EMI noise diagnosis," *IEEE Trans. Power Electron.*, vol. 20, no. 4, pp. 974–982, Jul. 2005.
[14] D. Zhao, J. A. Ferreira, A. Roc'h, and F. Leferink, "Common-mode DC-bus filter design for variable-speed drive system via transfer ratio measurements," *IEEE Trans. Power Electron.*, vol. 24, no. 2, pp. 518–524, Feb. 2009.
[15] K. Borisov, H. L. Ginn, and A. M. Trzynadlowski, "Attenuation of electromagnetic interference in a shunt active power filter," *IEEE Trans. Power Electron.*, vol. 22, no. 5, pp. 1912–1918, Sep. 2007.

Shuo Wang (S'03–M'06–SM'07) received the B.S.E.E. degree from Southwest Jiaotong University, Chengdu, China, in 1994, the M.S.E.E. degree from Zhejiang University, Hangzhou, China, in 1997, and the Ph.D. degree from the Center for Power Electronics Systems (CPES), Virginia Polytechnic Institute and State University (Virginia Tech), Blacksburg, in 2005.

He has been with electrical power systems, GE aviation systems, Vandalia, OH since 2009. He was a Research Assistant Professor at the Center for Power Electronics Systems, Virginia Tech from 2005 to 2009. He holds four U.S. patents and has another two pending. He has published more than seventy academic papers in IEEE TRANSACTIONS and IEEE conferences. His research interests include EMI/EMC in power electronics systems, high density power conversion, three-phase power conversion and inversion, motor drive, generator control and power systems.

Dr. Wang received the 2005 Best Transaction Paper Award from the IEEE TRANSACTIONS ON POWER ELECTRONICS and the William M. Portnoy Award for the best paper published in IEEE IAS Annual Conference in 2004. He is an Associate Editor for IEEE Transactions on Industry Applications.

Yoann Yorrick Maillet received the B.S. degrees in electrical engineering from Virginia Polytechnic Institute and State University (Virginia Tech), Balcksburg, in 2006, and the M.S. degree from the Center for Power Electronics Systems, Virginia Tech, in 2008.

Since 2008, he has been an Electrical Engineer in Converteam, Inc., Pittsburg, PA. His current research interests include passive electromagnetic interference filter design, and integrated EMI choke for CM and DM suppression.

Fei (Fred) Wang (S'85–M'91–SM'99–F'10) received the B.S. degree from Xi'an Jiaotong University, Xi'an, China, in 1982, and the M.S. and Ph.D. degrees from the University of Southern California, Los Angeles, in 1985 and 1990, respectively, all in electrical engineering.

From 1990 to 1992, he was a Research Scientist in the Electric Power Laboratory, University of Southern California. In 1992, he joined the GE Power Systems Engineering Department, Schenectady, NY, as an Application Engineer. From 1994 to 2000, he was a Senior Product Development Engineer with GE Industrial Systems, Salem, VA. From 2000 to 2001, he was the Manager of the Electronic and Photonic Systems Technology Laboratory, GE Global Research Center, Schenectady, and Shanghai, China. During 2001, he was a Research Associate Professor in the Center for Power Electronics Systems (CPES), Virginia Polytechnic Institute and State University, Blacksburg, where he became an Associate Professor in 2004 and the CPES Technical Director during 2003. In 2009, he joined The University of Tennessee and Oak Ridge National Laboratory, Knoxville, as the Condra Chair Professor in power electronics. His current research interests include power electronics, power systems, controls, electric machines, and motor drives.

Dushan Boroyevich (S'81–M'82–SM'03–F'06) received the Dipl. Ing. degree from the University of Belgrade, Belgrade, Yugoslavia, in 1976, the M.S. degree from the University of Novi Sad, Yugoslavia, in 1982, and the Ph.D. degree from Virginia Polytechnic Institute and State University (Virginia Tech), Blacksburg, in 1986.

From 1986 to 1990, he was an Assistant Professor and the Director of the Power and Industrial Electronics Research Program, Institute for Power and Electronic Engineering, University of Novi Sad, where he was also the Head of the Institute. He was an Associate Professor in Bradley Department of Electrical and Computer Engineering, Virginia Tech, where he is currently the American Electric Power Professor and a Co-Director of the Center for Power Electronics Systems. His research interests include multiphase power conversion, electronic power distribution systems, power electronics systems modeling and control, and multidisciplinary design optimization.

Dr. Boroyevich is the recipient of the IEEE William E. Newell Power Electronics Technical Field Award.

Rolando Burgos (S'96–M'03) received the B.S. degree in electronics engineering, the Electronics Engineering Professional degree, and the M.S. and Ph.D. degrees from the University of Concepción, Concepción, Chile, in 1995, 1997, 1999, and 2002, respectively, all in electrical engineering.

In 2002, he was a Postdoctoral Fellow in the Center for Power Electronics Systems, Virginia Polytechnic Institute and State University (Virginia Tech), Blacksburg, where he was a Research Scientist in 2003 and a Research Assistant Professor in 2005. In 2009, he joined the U.S. Corporate Research Center, ABB, Inc., Raleigh, NC, where he is currently a Power Electronics Consulting R&D Engineer. His research interests include multiphase and multilevel power conversion, stability of ac and dc power electronics systems, hierarchical modeling, control theory, and the synthesis of power electronics conversion systems.

Dr. Burgos is a member of the IEEE Power Electronics Society, the IEEE Industrial Electronics Society, the IEEE Industry Applications Society, and the IEEE Power Engineering Society. He is also the Secretary of the Committee on Simulation, Modeling and Control of the IEEE Power Electronics Society.